Dislocation mediated variant selection for secondary twinning in compression of pure titanium

Shun Xu, László S Tóth, Christophe Schuman, Jean-Sébastien Lecomte, Matthew R Barnett

Dislocation mediated variant selection for secondary twinning in compression of pure titanium

Shun Xu[1,2], Laszlo S. Toth[1,2], Christophe Schuman[1,2], Jean-Sébastien Lecomte[1,2], Matthew R. Barnett[3]

[1]Laboratoire d'Etude des Microstructures et de Mécanique des Matériaux (LEM3), CNRS UMR 7239,Université de Lorraine, F-57045 Metz, France

[2]Laboratory of Excellence on Design of Alloy Metals for low-mAss Structures (DAMAS), Université de Lorraine, France

[3] ARC Centre for Excellence for Design in Light Metals, Institute for Frontier Materials, Deakin University, Geelong, Australia

Abstract

By compression along the normal direction of rolled pure titanium sheet, primary $\{11\bar{2}2\}$ type compression twins were observed, followed by secondary $\{10\bar{1}2\}$ extension twins. The latter can be classified into three groups according to their misorientation with respect to the parent matrix grains: 41.34° around $<5\bar{1}\bar{4}3>$ (Group I), 48.44° around $<\bar{5}503>$ (Group II), and 87.85° around $<7\bar{4}\bar{3}3>$ (Group III). The experimental observations revealed the following activity frequency of these groups: Group II is the most frequent followed by Group I, and only a few secondary twins can be seen for Group III. When the classical Schmid factor (SF) analysis is applied, the smallest activity is predicted for Group III, in agreement with the experimental observations. However, the SF based criterion fails to distinguish between Group I and Group II variants. Similarly, the twin-shear accommodation model proposed earlier for titanium [Qin and Jonas, Acta Mater. 75 (2014) 198-211] is not effective because mainly Group III variants accommodate the secondary twins by prismatic slip. A possible explanation can be based on the smallest inclination angle of the secondary twinning habit plane with respect to the primary one, proposed by Barnett et al. [Acta Mater. 56 (2008) 5-15] which clearly favors Group II. It cannot make distinction between variants of the same group but can predict the right variants if complemented with the SF criterion. In the present work a new approach is proposed in order to disclose the preference for Group II variant over Group I. It is based on the special twinning geometry that applies to Group II; the intersection line of the primary and secondary twin planes lies in an active prismatic plane in the primary twin. Consequently, dislocation reactions are possible for the selection of secondary twin variant in Group II. Namely, prismatic <**a**> type dislocations in the primary twin can produce partial dislocations

that activate the corresponding secondary twin variant. Nevertheless, a further selection rule has to be applied to choose one out of the two possible Group II variants; this is based on the higher Schmid factor of the two secondary variants. By contrast, pyramidal dislocations would be required for the formation of Group I twins, which is less likely due to their relatively high critical resolved shear stress.

Keywords: Titanium; EBSD; twinning; secondary twinning; variant selection

1. Introduction

The wide application of hexagonal close packed (HCP) metals such as α-titanium, magnesium and zirconium in aerospace technology, automotive and nuclear industry requires a deep understanding of their deformation mechanisms. These metals are characterized by a large variety of possible slip systems [1-3]: basal <**a**> $\{0002\}<11\bar{2}0>$, prismatic <**a**> $\{10\bar{1}0\}<11\bar{2}0>$, pyramidal <**c**+**a**> $\{10\bar{1}1\}<11\bar{2}3>$, and pyramidal <**a**> $\{10\bar{1}1\}<11\bar{2}0>$. Besides slip, deformation twinning plays a significant role in the plastic deformation to accommodate the strain along c-axis of the crystal, especially at low temperatures [4] and high strain rates [5]. At room temperature, several twinning modes have been observed in α-titanium [6]. Extension twins including $\{10\bar{1}2\}<\bar{1}011>$, $\{11\bar{2}1\}<\bar{1}\bar{1}26>$ and $\{11\bar{2}3\}<\bar{1}\bar{1}22>$ induce a positive strain along the c-axis of the parent grain, while contraction twins, such as $\{11\bar{2}2\}<11\bar{2}\bar{3}>$, $\{11\bar{2}4\}<22\bar{4}3>$ and $\{10\bar{1}1\}<10\bar{1}\bar{2}>$, cause reduction along the c-axis [7].

The large reorientation caused by primary twinning can reposition initially non-active twinning systems of the parent grain into more favourable orientation, promoting secondary twinning inside the primary twins. The following secondary twin systems are reported in magnesium alloys: $\{10\bar{1}2\}$ twins in $\{10\bar{1}1\}$ primary twins [8-10], and $\{10\bar{1}2\}$ twins in primary $\{10\bar{1}2\}$ twins [11, 12]. The former can readily appear during uniaxial deformations [13, 14]. Barnett et al. [8] reported that the $\{10\bar{1}1\}-\{10\bar{1}2\}$ double twin variants that are favoured are those that correspond to minimum compatibility strain in the primary $\{10\bar{1}1\}$ twins. Martin et al. [9] found that the secondary twin variants having the greatest potential for growth and with the highest resolved shear stress are most favourable during the selection of secondary twin variants. $\{10\bar{1}2\}-\{10\bar{1}2\}$ double twins were found in AZ31 in uniaxial deformation at 77K, possibly due to the absence of non-basal slip at low temperature, while they did not appear at room temperature deformation where non-basal slip can take place [11]. Wang et al. [15-17]

declared nucleation mechanism of twinning in HCP metals by using simulation. Beyerlein et al. rationale selection based on nucleation via dislocation reaction at the primary twin interface [18]. In pure titanium, $\{11\bar{2}2\}$ and $\{10\bar{1}2\}$ twins are most frequently observed at room temperature [6, 19, 20], compared to other twinning systems. Christian and Mahajan put forward that a low shear and a small shuffling facilitates the formation of these twins [4]. Several compression tests were carried out on commercially pure titanium to study secondary $\{10\bar{1}2\}$ extension twinning inside primary $\{11\bar{2}2\}$ compression twins in Refs. [21-23]. Jonas et al. [10, 23, 24] recently employed strain accommodation to evaluate the selection of twin variants. In their work, the generation of secondary twins was explained by inspecting several deformation modes in the adjacent parent grains to accommodate the shear induced by the secondary twins [23]. It was proposed that those secondary twin variants are initiated for which the strain can be accommodated the most easily by prismatic or basal glide in the parent. The displacement gradient tensor of the shear operating in the secondary twin frame was transformed into the crystal fame of the neighboring parent grain to identify the slip system in the parent grain that can accommodate the twinning shear displacement in the twin boundary region. Wang et al. [25, 26] considered twinning accommodated by twinning on the other side of a boundary. They employed the Luster-Morris parameter [26-28] defined by $m'=\cos\psi \cdot \cos\kappa$, where ψ is the angle between the normal of the two planes and κ is the angle between two shear directions of the systems, which can be used to quantify the compatibility of accommodating slip or twinning. Recently, the preferred secondary twins were found with a misorientation relation of 41° around a $<5\bar{1}\bar{4}3>$ axis compared to the matrix in commercially pure titanium subjected to cold-rolling [29]. The activation of secondary twinning induced by channel-die compression was recently reported and found to be reasonably consistent with a simplified Schmid factor (SF) criterion [30].

There are evidently a range of findings and interpretations in the literature and the present work aims to test their applicability to secondary $\{10\bar{1}2\}$ twining within primary $\{11\bar{2}2\}$ twins in uniaxially compressed pure titanium. It is found in the present work that the only SF based and also the accommodation based secondary twin selection criteria [23] cannot explain the experimental observations. However, the habit plane orientation based criterion - originally proposed for magnesium [8] - applies also to titanium; i.e., it selects the right group (Group II). It does not, however, select the right variant within the group. The main contribution to the topic in the present work is a new criterion which is also able to reproduce the experimental secondary twinning activity. It is based on the special geometry that applies to Group II

secondary twins in titanium: there is a common intersection line between three planes: the active prismatic plane in the primary twin and the primary and secondary twin planes. This special geometry makes possible dislocation reactions that are necessary for producing the partial dislocations of the secondary twin. Nevertheless, the Schmid factor criterion is still needed to choose between the two possible Group II $\{10\bar{1}2\}$ twins variants inside the $\{11\bar{2}2\}$ primary twins.

2. Experimental procedure

In the current study, the material used was rolled commercially pure titanium T40 sheet (ASTM grade 2) with a thickness of 1.5 mm. The composition is given in Table 1. It is generally understood that deformation twinning is more active with a larger grain size [31-33]. Therefore, samples with a large grain size were prepared by annealing in a vacuum furnace at 800°C for 2 h, leading to a fully-recrystallized microstructure. By using a Zwick 120T machine, the samples were deformed at room temperature with 8.1% reduction at a strain rate of $1\times10^{-3}s^{-1}$. The compression direction (CD) was parallel to ND (normal direction). After compression, the rolling plane of the compressed sample was ground with SiC papers of grits from 1200# to 4000#. Finally, electrolytic polishing was conducted at 35 V and 5°C for 5 s in a solution of 10% perchloric acid and 90% methanol.

Electron backscatter diffraction (EBSD) measurements were performed on a JEOL 6500F field emission gun (FEG) and on a JSM 6490 SEM microscope equipped with an EBSD camera and the AZtec acquisition software package (Oxford Instruments). The sample was tilt by an angle of 70°. A voltage of 20 kV was used with a working distance of 15 mm. A step size of 5 μm was adopted to detect the texture of the initial material. For more detailed examination of twins, EBSD patterns were acquired on the deformed sample at a step size of 0.5 μm. The texture was analysed with the help of the JTEX software [34] and presented in pole figures.

Crystal plasticity simulations were carried out to obtain information on the required slip systems for accommodating the twin shears that are produced by the secondary twins at primary twin boundary in the parent grain. The fully imposed Taylor approach is suitable for such calculation in which the twin shear is imposed on the parent orientation. The approach based on rate sensitive slip proposed in Ref. [35] was used for this purpose. The results are reported in Section 4.2.

3. Results

3.1 Microstructure in the initial and deformed states

Fig. 1 presents the microstructure of the initial material in form of EBSD inverse pole figure (IPF) where the ND axis was projected with the shown color code. The material was fully recrystallized with an average grain size of ~160 µm and presented no twins. RD and TD represent the rolling and transverse directions, respectively. Fig. 2a displays the texture of the material in $\{0002\}$, $\{11\bar{2}2\}$ and $\{10\bar{1}0\}$ pole figures obtained from Fig. 1. The rolling symmetry appears well satisfied by these EBSD measurements meaning that the texture can be considered to be representative (the number of grains is 1880 in the map in Fig. 1).

As can be seen in Fig. 2a, the c-axes were oriented ±40° from the ND towards the TD, which is a typical texture of a rolled titanium sheet - retained after recrystallization - and is caused by the activities of diverse slip modes during rolling. It has been reported that the texture with basal poles tilted from the ND to the TD for titanium and zirconium results from the dominating $\{10\bar{1}0\}<11\bar{2}0>$ prismatic and $\{0002\}<11\bar{2}0>$ basal slip, while in cadmium and zinc the component with basal poles tilted from the ND towards the RD is attributed to $\{11\bar{2}2\}<11\bar{2}\bar{3}>$ pyramidal and $\{0002\}<11\bar{2}0>$ basal slip. In magnesium, $\{0002\}<11\bar{2}0>$ basal slip assists the formation of the basal texture (c axis parallel to the ND), where the c/a ratio is close to 1.633 [36-38].

The IPF EBSD map obtained on a sample after a compressive strain of 8.1% along the ND is shown in Fig. 3a and b. The main twin systems detected in this work are listed in Table 2. Boundaries with a tolerance of ±5° deviation from the axis and the angle are plotted. This enables detection of $\{11\bar{2}2\}$ and $\{11\bar{2}4\}$ compression twins as well as $\{10\bar{1}2\}$ and $\{11\bar{2}1\}$ extension twins. In Fig. 3b, random boundaries with misorientations larger than 5° are traced in black. The $\{11\bar{2}2\}$ compression twins are shown in green (64° rotations around $<\bar{1}100>$), while the $\{10\bar{1}2\}$ extension twins are depicted in red (87° misorientations around $<11\bar{2}0>$). The green lines correspond chiefly to primary $\{11\bar{2}2\}$ compression twins formed in the parent grains or secondary $\{11\bar{2}2\}$ compression twins in primary $\{10\bar{1}2\}$ twins. Red lines are typically primary $\{10\bar{1}2\}$ extension twins in the parent grains or secondary $\{10\bar{1}2\}$ extension twins in primary $\{11\bar{2}2\}$ compression twins. Yellow and pink lines correspond to $\{11\bar{2}1\}$ and $\{11\bar{2}4\}$ twins, respectively.

Fig. 3c shows the next-neighbour grain to grain misorientation distribution and reveals that there are strong peaks at ~65° and ~87°, which can be attributed to the formation of $\{11\bar{2}2\}$

and $\{10\bar{1}2\}$ twins, respectively. A large number of primary twins form in the parent grains and many secondary twins can be seen within these primary twins. The two peaks identified as $\{11\bar{2}2\}$ twins and $\{10\bar{1}2\}$ twins in Fig. 3c belong to both primary and secondary twins (no distinction is made). Another peak can be seen between 40° and 50°. This angle is not listed in Table 2 because it arises from boundaries between $\{11\bar{2}2\}-\{10\bar{1}2\}$ or $\{10\bar{1}2\}-\{11\bar{2}2\}$ double twins and the parent matrix (see more in Section 3.3). In the present study, $\{10\bar{1}2\}-\{11\bar{2}2\}$ double twins were not observed while a large amount of $\{11\bar{2}2\}-\{10\bar{1}2\}$ double twins were detected. The $\{11\bar{2}1\}$ extension and $\{11\bar{2}4\}$ compression twins do not produce peaks in Fig. 3c at ~35° and ~77°, respectively, because of their small frequency. This is consistent with the characteristics of the texture because such initial texture favours the formation of $\{11\bar{2}2\}$ twins in ND compression [23].

3.2 Misorientation between a secondary twin and its parent grain

For each primary $\{11\bar{2}2\}$ compression twin, there are six possible secondary $\{10\bar{1}2\}$ extension twin variants. Therefore, comparing parent grain orientations to double-reoriented regions, there are 36 possible combinations. The misorientation between a secondary $\{10\bar{1}2\}$ twin originating from a primary $\{11\bar{2}2\}$ twin and its parent grain was determined by rotating the orientation of the parent grain around the respective normal directions of primary and secondary twinning planes by an angle of 180° in each case. After these rotations, the 12 symmetry operations of the hexagonal lattice were applied (six times 60° around the c-axis with 0° and 180° rotations around one a-axis) and the minimum misorientation angle was computed between the orientation matrix of the parent and the 12 equivalent matrices of the secondary twin. The 36 independent possibilities are listed in Table 3; they can be divided into three groups based on their axes and minimum disorientation angles with respect to the parent grain. In each primary $\{11\bar{2}2\}$ twin, there are two secondary variants for each group. In Table 4 the three groups are defined; each group of secondary twins has the same number of 12 variants.

Fig. 4 displays one example of primary and secondary twin variants for each of the three groups listed in Table 4 in form of EBSD orientation maps and pole figures. For each group, the {0002} poles of the parent grains are located in the vicinity of the center of the pole figure, which enables $\{11\bar{2}2\}$ twinning to be readily activated. A common characteristic between the

three groups is that primary twinning takes the c-axis of the twinned part away from the center region. As for the secondary twins, the c-poles are returned near the center region for Groups I and II while those for group III variants, they are oriented in a position largely deviating from the ND.

The $\{11\bar{2}2\}$ pole figures in Fig. 4 display both the poles of the parent and the selected primary twin. The common pole belongs to the primary twin plane and is labeled by a small blue circle. A line segment is drawn in the figure perpendicular to the projected twin plane normal direction. This line segment lies both in the RD-TD and in the primary twin planes, so it indicates the orientation of the twin boundary line in the micrograph. Indeed, for all three groups, the orientation of this boundary line is nearly parallel to the twin-platelet (it is indicated with PTB and also traced in the IPF micrographs by white line)[1]. Similar construction indicates the orientation of the secondary twin boundary in the $\{10\bar{1}2\}$ pole figures where the secondary twin plane normal is indicated with a red circle and the twin boundary with STB.

3.3 Texture variations due to primary and secondary twinning

Using the EBSD grain orientation data obtained for the matrix grains as well as for the twins, it is possible to visualize the changes that occur in the texture due to twinning. The result of such analysis is displayed in Fig. 2b in forms of {0002} pole figures, separately for the matrix grains, for the primary $\{11\bar{2}2\}$ twins and for the secondary $\{10\bar{1}2\}$ twins. The parent grains and primary twins included in the texture are those where secondary twins were seen. The initial texture with the c-axes aligned near to the center of the pole figure favours the activation of $\{11\bar{2}2\}$ twinning by compression in the ND direction. Primary $\{11\bar{2}2\}$ twinning reorients the basal plane of the matrix by ~64° around a $<1\bar{1}00>$ direction. As a result, the basal poles of the primary twins are located away from the ND as shown in Fig. 2b for the primary twins. The stress state favourable for primary $\{11\bar{2}2\}$ twinning in the parent grains also supports the occurrence of secondary $\{10\bar{1}2\}$ twinning in the identified primary twins. Due to secondary $\{10\bar{1}2\}$ twinning, the basal poles of the primary twins are rotated by ~86° around a $<11\bar{2}0>$ axis. In the present case, this leads to basal poles in the center of the pole figure. With

[1] Note that perfect parallel is only expected for very thin platelets because for thick twins the growth rate of the twin boundary is generally not uniform. Usually lenticular shapes appear because of the pile-up of twinning dislocations against the grain boundaries.

reference to Fig. 4, this suggests that Group I and/or II double twins are dominant because these types return the c-axis to the ND.

3.4 Classification of the detected secondary {10-12} twins

As displayed in Table 4, the 36 possible $\{11\bar{2}2\} - \{10\bar{1}2\}$ double twin variants involve three groups. In the present statistics, 425 secondary $\{10\bar{1}2\}$ twins were detected by EBSD. For this population of secondary twins, the frequency of the three groups is shown in Fig. 5a. This figure indicates clearly that Group II (i.e., $<\bar{5}503> 48.44°$) accounts for 85.6% of the twin population. Only 10.6% and 3.8% of the secondary twins belong to Group I and Group III, respectively. Group II secondary twin variants are clearly preferentially selected in the primary twins.

4. Discussion

4.1 A Schmid factor based evaluation of the secondary {10-12} twins

The Schmid factor (SF) is conveniently used as a reference point for examining variant selection. It is based on the idealized hypothesis that the stress direction in a grain is exactly the same as the one applied on the whole sample. From this hypothesis one obtains the following simple formula for the SF:

$$SF = \cos\lambda \cdot \cos\theta \tag{1}$$

Here λ is the angle between the loading direction (LD) and the twin plane normal (TPN) while θ is the angle between the LD and the twin shear direction (SD). It is expected that twin variants with high SFs will tend to be more active.

It is helpful to normalize the SF [39]; all twinning SF values in a given grain are divided by the highest SF value found in that grain to obtain the normalized Schmid factor, $NSF(i)$:

$$NSF(i) = \frac{SF(i)}{SF_{\max}}, \quad i = 1...6 \tag{2}$$

The maximum possible value of $NSF(i)$ is 1. The distribution of the *NSF* values of the 425 secondary twins measured in the present study is shown in Fig. 5b. As indicated in the figure, 93.4% of the twins have an *NSF* factor higher than 0.8. Only one secondary twin variant is activated in most primary twins. 4.5% of the secondary twins are found in the primary twins where two variants are activated. A colour code is used in Fig. 5b to identify twins of different categories starting from *NSF* = 0.8. Red colour indicates that the highest SF variant is activated,

so the SF rule is respected. For a few cases marked by red, the second highest NSF variant is also active in the same primary twin - they are counted in the other NSF intervals according to their NSF factors (between [0.8, 0.9) and [0.9, 1)). There was no case when the first three highest NSF variants were all active in the same primary twin. The blue coloured column indicates the proportion of twins that are present in the material with $NSF < 1$, moreover, the variant corresponding to $NSF = 1$ is absent in those primary twins. The meaning of the green colour is similar: it shows the population of twins that have even smaller *NSF* factors, without the presence of other twin variants with higher *NSF* in those primary twins. Thus, the blue and green colour columns together indicate the proportion of twins that do not obey the classical Schmid law. Totally, we can identify 49.3% of the secondary twin variants that do not obey Schmid law.

Fig. 5b also indicates the proportion of twins belonging to the three possible groups defined in Table 4. Only Groups I and II appear in the coloured regions because Group III is present only with *NSF* factors less than 0.8. As can be seen from Fig. 5b, Group II is particularly disobeying the Schmid law because it represents (count in the blue and green colour columns) 47.5% of the total twins and 96.2% of the non-Schmid twins. The non-Schmid part of Group I is 1.9% and for Group III it is 3.8% of the total population.

Fig. 5b is the experimental situation, so that it should be compared to the theoretical prediction based on the Schmid factors by respecting the activation of high NSF twin systems. For this purpose a full analysis was carried out considering all possible secondary twins that potentially can form in the detected primary twins. We consider only those variants that carry the first and second highest Schmid factors. Smaller SF variants are omitted because generally one or two variants appear in a primary twin. Fig. 5c shows the result of such analysis: Group III variants constitute only 0.5% of all possible variants, while Group I and II account for 50.2% and 49.3%, respectively. The small population of group III twins concurs with the experimental observations, so their absence can be convincingly attributed to their relatively low SFs. However, our analysis predicts similar proportions for Group I and II twins. This is not consistent with the experiment: Group II twins alone represent 85.6% of the total population of the detected secondary twins (Fig. 5a). Even though the active secondary twin variants carry high SFs in [30], this classical law is found to be invalid in explaining the occurrence of secondary twinning in our work. In [29], secondary twins belonging to Group I are discovered to be commonly generated.

Since only one secondary twin variant is activated in majority of the primary twins, it is a simple matter to simulate the effect of activating different secondary twin variants on the secondary twin textures. The orientations of possible secondary twins were artificially calculated within the detected primary twins to reveal particular secondary twin variants. Each group includes two secondary twin variants. The reorientation of the texture by the secondary twin variant with a higher SF is shown in Fig. 2c. The c-poles of the secondary twins induced by Groups I and II variants are located close to the center of the pole figure, which is similar to the experimental result. Those secondary twins by Group III variants are largely misaligned with the observed secondary twins as indicated in Fig. 2c. However, the other variant carrying a lower SF in each group reorients the texture as presented in Fig. 2d, which reveals that these secondary twins are not in agreement with the detected results. This is true for the three groups. Therefore, the texture evolution illustrates that the selection between two secondary twin variants in the same group is controlled by the SF criterion. Only one variant is favored for Group I and Group II, respectively. It is clear that a Schmid factor based selection rule is only effective to resolve the absence of Group III variants as well as one variant in Group I, and also one in Group II.

In conclusion, it follows from the above Schmid factor analysis that there remain only two possible variants that can explain the experimental observation. They are: the higher Schmid factor cases in Groups I and II. Therefore, further selection rule is needed because Group II is much more favored than Group I. This will be established in Section 4.4 with the help of dislocation mediated mechanisms.

4.2 Accommodation in the parent grain

The next step is then to examine the applicability of the recently proposed accommodation based selection criterion [23] on our measurements. In Ref. [23], the displacement gradient tensor of a possible secondary twinning variant was transformed into the neighbor mother grain. The components of the obtained tensor correspond to different slip systems. Then that secondary twin variant was admitted which was the best compatible with the displacement gradients produced by basal or prismatic slip in the neighbor grain.

In our analysis we applied this approach in the following way. First, for each experimentally observed primary twin orientation containing secondary twins, we expressed the velocity gradients of the shears corresponding to the six possible secondary twins in the sample reference system of the EBSD measurement. Then these velocity gradients were

imposed on the mother grain, one by one. All possible slip families of h.c.p. crystals were considered in the mother grains for possible accommodation of the secondary twin shears; they are listed in Table 5. The CRSS values of these systems were taken from Ref [40] where the same material composition was studied. The single crystal plasticity problem was solved to obtain the necessary slip distribution within the mother grain by employing the full constraints conditions of crystal plasticity with viscoplastic slip according to the approach published in [35]. The value of the strain rate sensitivity index for slip was m=0.05. The calculation was done in the sample reference system in full constraints conditions, which is the only possible approach that can be considered at a grain boundary between the primary twin and the mother grain. The resulting slip distribution was examined for each secondary twin variant. Note that this accommodation approach is more rigorous than the one employed in [23], because the accommodation is possible for any shear caused by secondary twins and produces precise values for the slips in the mother grain.

The simulation result is displayed in Fig. 5d: twinning shear in Group I is mainly accommodated by <c+a> pyramidal-1 slip. For a small fraction of cases, basal and prismatic slip are the most active. For Group II - which is the most frequently observed experimentally - basal slip is the major accommodating slip mode, in a few cases prismatic slip, and in 22% <c+a> pyramidal-1 slip. Group III requires mostly prismatic slip (80%) and in a few cases basal slip, <c+a> pyramidal-1 as well as <a> type pyramidal. The accommodation by <c+a> pyramidal-2 slip is very rare. Focusing on the most frequent experimental case - Group II - one can see that the proposition of prismatic slip accommodation (Ref. [23]) is not valid for our experiments. The simulations confirm mostly basal-slip accommodation. Accommodation by prismatic slip is predicted for Group III - which is rare in the experiments. Therefore, the selection criteria based on accommodation by prismatic slip is not validated by our experiments and simulations.

4.3 Twin shape effect

The secondary twin shape is enforced by the shape of primary twins. The angles between the primary and secondary twin planes for the three groups of secondary twin variants are shown in Table 6. It can be seen that the angle between the primary and secondary twin planes belonging to Group II variants is smaller than that for other groups. Barnett et al. [8] proposed that the variant presenting the smallest angle is favored for energy reasons. Their work was carried out for Mg. When applying this criterion to our present Ti case, it is clear that Group II is correctly favored; however, the angle is the same for the two secondary twin variants within Group II, so it is not possible to favor one of them. However, combining Barnett's

criterion with the larger Schmid factor case, the right variant can be selected, in agreement with the experimental results. Nevertheless, a new selection mechanism is also proposed in Section 4.4 below, which is mediated by dislocations in the primary twin and also able to account for the experimental observations for the frequency of secondary twins.

4.4 Dislocation mediated mechanism

The particularity of the secondary extension twins is that their c-axes are nearly perpendicular to the primary twin c-axis. A consequence of this is a large difference in the stress state between the twinned and matrix grain regions. Indeed, crystal plasticity simulations show that the stress state in a grain can be very different from the macroscopic applied stress [41]. Internal stresses arising from the twins and from the neighboring grains can also play a significant role [42, 43]. These are probably responsible for the variation in NSFs for active Group II twins, but the effect is unlikely capable to explain the striking difference between Group I and II variants. In looking elsewhere for an explanation without going into detailed crystal plasticity simulations, we examine dislocation reaction based mechanism, using the principles developed for magnesium in Ref [18].

As discussed above, in each primary $\{11\bar{2}2\}$ twin, three distinct secondary twin variants can be created which can be characterized by the misorientation between the parent grains and secondary twins; they are referred to Group I, II and III (Table 4). Fig. 6 shows the geometrical relationship between a selected primary $(11\bar{2}2)$ twin plane and the possible six secondary twin planes within the HCP unit cell of the primary twin. For Group I, the common direction shared by the primary twin plane and the planes of two Group I variants lies along j-k in Fig. 6c and along m-n in Fig. 6d, respectively. It is apparent from the figure that these two common directions belonging to Group I are both non-parallel to any prismatic plane in the primary twin. However, the common directions in Fig. 6e and Fig. 6f between the primary twin plane and the planes of two Group II variants (along C-f and along A-d, respectively) are both located in prismatic planes in the primary twin. The same features are also valid for Group III variants as shown in Fig. 6g and 6h. Thus, the primary plane, the secondary twin planes and a prismatic plane intersect along the same direction for Group II and III variants. However, Group III will not be considered in the following because their occurrence can be neglected due to their very low SFs (see preceding section).

The Miller indices of the intersection lines between the primary twin plane and three groups of secondary twin planes, as well as of the corresponding prismatic planes in the primary twin

are listed in Table 7. As determined graphically above, for Group II twins, the common direction is in a prismatic plane, offering good geometrical conditions for the possible dissociation of prismatic <**a**> dislocations [44, 45]. <**a**> type prismatic glide $\{10\bar{1}0\}<11\bar{2}0>$ is favored for titanium and zirconium (γ<1.633) [46, 47]. Thus, the nucleation of Group II twins could conceivably originate from reactions of <**a**> type prismatic dislocations in the primary twin that glide into the primary twin boundary. Such reactions are facilitated by the shared axis of the prismatic slip and Group II twinning planes lying in the primary twin boundary.

A similar argument has been developed in detail for secondary twinning in magnesium by Beyerlein et al. [18]. According to their proposal, the reaction of basal <**a**> dislocations with residual dislocations in the primary $\{10\bar{1}1\}$ boundary can lead to the formation of $\{10\bar{1}2\}$ twinning dislocations. A structure requirement for this reaction is that the basal dislocation, the primary twin and secondary twin share a common zone axis. As mentioned above, this structure requirement is met in the case of Group II twinning but for prismatic <**a**> slip, not for basal <**a**> slip, as for the magnesium case. In the present case, the primary $\{11\bar{2}2\}$ twin domains are indeed favourable for prismatic <**a**> slip by compression along the ND. When such slip is active, the nucleation of the secondary twin variants can be understood by the following reactions analogous to those proposed by Beyerlein et al. [18] for Mg:

$$\text{Step (1):}\quad 1/3[\bar{2}110] \rightarrow b_r^1 + b_{tw}^{\{11\bar{2}2\}},$$

$$\text{Step (2):}\quad 1/3[\bar{2}110] + b_r^1 \rightarrow b_r^2 + b_{tw}^{\{10\bar{1}2\}},$$

where b_r^i (i=1,2) are residual dislocations. Step (1) was proposed by Mendelson [44] and step (2) can be understood to arise once further incoming lattice dislocations react with the residual from the first reaction to produce secondary twinning dislocations.

Looking into the Group I secondary twin configurations with respect to the primary twins, a dislocation dissociation mechanism similar to the one proposed for Group II twins cannot be found. The reason is that the secondary twins belonging to Group I do not benefit from common zone axis in the same way as in Group II variants. They intersect with the primary twin boundary along directions that are not parallel to any prismatic or primary twin planes (see Fig. 6c and d). Moreover, the common lines do not correspond to any crystal direction among the available HCP slip planes and the primary twin boundary. It is also true that for a possible dislocation reaction, <**c+a**> type dislocations would be needed which are hard to activate in

titanium. Therefore, Group I twins can be expected to be much more difficult to form compared to Group II, as is observed.

In order to confirm the activation of the associated prismatic slip in the primary $\{11\bar{2}2\}$ twin with the preferred secondary $\{10\bar{1}2\}$ Group-II twin, a sample was pre-polished and deformed under compression, followed by the observation of slip traces with the help of secondary electron imaging. Primary $\{11\bar{2}2\}$ and secondary $\{10\bar{1}2\}$ twins were detected as shown in Fig. 7a. Clear slip traces were found in the area identified in the orientation map in Fig. 7a; the corresponding secondary electron image is displayed in Fig. 7b. The Miller indices of the primary and secondary twin systems were $(\bar{1}\bar{1}22)[\bar{1}\bar{1}2\bar{3}]$ and $(0\bar{1}\bar{1}2)[01\bar{1}\bar{1}]$, respectively (all indices are expressed in the primary twin reference frame). Therefore, this secondary twin belongs to Group II. The expected slip-line directions in the observation plane corresponding to the three prismatic planes in the primary twin were computed and plotted in Fig. 7c. As can be seen, one prismatic plane is parallel to the slip lines in Fig. 7b; the $(10\bar{1}0)$ (identified with a blue line in Figs. 7b and c). Out of the three possible prismatic planes only the observed $(10\bar{1}0)$ plane satisfies the Group II configuration. Therefore, the presented geometry corresponds to the preferred group; Group II. There are two variants within Group II, out of which the highest Schmid factor variant is preferred, see our proposed model above. Indeed, the higher Schmid factor variant can be seen in Fig. 7 with a Schmid factor of 0.42 in contrast to the other variant which is 0.27.

In summary, our proposed model for explaining the experimental frequency of secondary twinning in compressed titanium is the following. The Schmid factor analysis eliminated four variants out of the six, so there remained only two; one in Group I and one in Group II. Between these two, the prismatic-dislocation mediated variant is active in Group II based on the common intersection of a prismatic plane in the primary twin and the twin planes of the primary twin and the secondary twin which makes possible the creation of partial dislocations for the active secondary twin. Therefore, our selection variant is based both on Schmid factors and the dislocation mediated mechanism.

Finally, we note that the predominance of Group II variants in the present case differs from the finding in Ref. [29]**.** In that study, cold rolling was performed and Group I secondary twins were found to be dominant. This difference likely relates to the difference in stress states

between the present experiments and those in Ref. [29]. In plane strain rolling, prismatic slip is not favoured in the primary twin domain, so the present mechanism is not expected to be active.

5. Conclusions

An experimental study was conducted in the present work for the combination of primary $\{11\bar{2}2\}$ compression and secondary $\{10\bar{1}2\}$ extension twins that were formed during compression in a pure polycrystalline titanium along the ND. A detailed analysis of the detected 425 secondary $\{10\bar{1}2\}$ twins has led to the following conclusions:

1. The 36 possible secondary twin variants can be classified into three groups in terms of misorientations between the parents and secondary twins: Group I with a misorientation of 41.34° around axis $<5\bar{1}\bar{4}3>$, Group II with a misorientation of 48.44° around axis $<\bar{5}503>$ and Group III with a misorientation of 87.85° around axis $<7\bar{4}\bar{3}3>$. The EBSD statistics revealed that Group II are the most frequent (85.6%), while Group I and III variants were only present in a fraction of 10.6% and 3.8%, respectively.
2. Our Schmid factor based analysis showed that 93.4% of the detected secondary twins had normalized Schmid factors larger than 0.8, where principally only a single secondary twin variant was activated in the primary compression twins. A small fraction (4.5%) of the secondary twins was found in the primary twins where two variants were observed. There was a very large fraction of secondary twins (49.3%) which did not obey the Schmid law.
3. The Schmid factor analysis also showed that Group III twins had very low Schmid factors, leading to their low experimental frequency. However, the Schmid factor criterion has led to nearly equal theoretical frequencies for twin variants of Groups I and II, which was contradictory to the experimental observations.
4. The competition between two variants in the same group is controlled by Schmid factor. Only one variant in Group I and one variant in Group II is favoured.
5. The accommodation approach proposed earlier in Ref. [23] is not applicable to select the active secondary twin variant. Those variants that can be accommodated by prismatic slip belong to Group III which were not active in the experiment.
6. The prevalence of Group II secondary twins over Group I was possible to justify with dislocation dissociations based on the common direction between the primary and secondary twin planes and a prismatic plane observed for Group II. Group I secondary twins cannot be formed by a similar mechanism which explains their relatively low frequency.

Acknowledgements

This work was supported by the French State through the program "Investment in the future" operated by the National Research Agency (ANR) and referenced by ANR-11-LABX-0008-01 (LabEx DAMAS). S. Xu sincerely thanks Dr. J. Wang (University of Nebraska-Lincoln) for valuable advice. Dr. Y.D. Zhang (Université de Lorraine) is greatly appreciated for fruitful discussions. We really thank the reviewer for giving valuable suggestions.

References

[1] P.G. Partridge. The crystallography and deformation modes of hexagonal close-packed metals, Metall Rev. 12 (1967) 169-194.
[2] M.G. Glavicic, A.A. Salem, S.L. Semiatin. X-ray line-broadening analysis of deformation mechanisms during rolling of commercial-purity titanium, Acta Mater. 52 (2004) 647-655.
[3] S. Zaefferer. A study of active deformation systems in titanium alloys dependence on alloy composition and correlation with deformation texture, Mater Sci Eng A. 344 (2003) 20-30.
[4] J.W. Christian, S. Mahajan. Deformation twinning, Prog Mater Sci. 39 (1995) 1-157.
[5] A.T. Santhanam, R.E. Reed-Hill. The influence of strain rate dependent work hardening on the necking strain in α-titanium at elevated temperatures, Metall Trans. 2 (1971) 2619-2622.
[6] A.A. Salem, S.R. Kalidindi, R.D. Doherty. Strain hardening of titanium: role of deformation twinning, Acta Mater. 51 (2003) 4225-4237.
[7] W. Tirry, S. Bouvier, N. Benmhenni, W. Hammami, A.M. Habraken, F. Coghe, D. Schryvers, L. Rabet. Twinning in pure Ti subjected to monotonic simple shear deformation, Mater Charact. 72 (2012) 24-36.
[8] M.R. Barnett, Z. Keshavarz, A.G. Beer, X. Ma. Non-Schmid behaviour during secondary twinning in a polycrystalline magnesium alloy, Acta Mater. 56 (2008) 5-15.
[9] É. Martin, L. Capolungo, L. Jiang, J.J. Jonas. Variant selection during secondary twinning in Mg–3%Al, Acta Mater. 58 (2010) 3970-3983.
[10] S. Mu, J.J. Jonas, G. Gottstein. Variant selection of primary, secondary and tertiary twins in a deformed Mg alloy, Acta Mater. 60 (2012) 2043-2053.
[11] J. Jain, J. Zou, C.W. Sinclair, W.J. Poole. Double tensile twinning in a Mg-8Al-0.5Zn alloy, J Microsc. 242 (2011) 26-36.
[12] Z.-Z. Shi, Y. Zhang, F. Wagner, T. Richeton, P.-A. Juan, J.-S. Lecomte, L. Capolungo, S. Berbenni. Sequential double extension twinning in a magnesium alloy: Combined statistical and micromechanical analyses, Acta Mater. 96 (2015) 333-343.
[13] M.R. Barnett. Twinning and the ductility of magnesium alloys: Part II."Contraction" twins, Mater Sci Eng A. 464 (2007) 8-16.
[14] D. Ando, J. Koike, Y. Sutou. Relationship between deformation twinning and surface step formation in AZ31 magnesium alloys, Acta Mater. 58 (2010) 4316-4324.
[15] J. Wang, I.J. Beyerlein, J.P. Hirth. Nucleation of elementary {-1011} and {-1013} twinning dislocations at a twin boundary in hexagonal close-packed crystals, Model Simul Mater Sci Eng. 20 (2012) 024001.
[16] J. Wang, J.P. Hirth, C.N. Tomé. (-1012) Twinning nucleation mechanisms in hexagonal-close-packed crystals, Acta Mater. 57 (2009) 5521-5530.
[17] J. Wang, R.G. Hoagland, J.P. Hirth, L. Capolungo, I.J. Beyerlein, C.N. Tomé. Nucleation of a (-1012) twin in hexagonal close-packed crystals, Scr Mater. 61 (2009) 903-906.
[18] I.J. Beyerlein, J. Wang, M.R. Barnett, C.N. Tome. Double twinning mechanisms in magnesium alloys via dissociation of lattice dislocations, Proc R Soc A Math. 468 (2012) 1496-1520.
[19] S. Xu, C. Schuman, J.-S. Lecomte. Accommodative {10-12} twins at high angle grain boundaries in rolled pure titanium, Scr Mater. 116 (2016) 152-156.
[20] Y.B. Chun, S.H. Yu, S.L. Semiatin, S.K. Hwang. Effect of deformation twinning on microstructure and texture evolution during cold rolling of CP-titanium, Mater Sci Eng A. 398 (2005) 209-219.
[21] C. Schuman, L. Bao, J. Sébastien Lecomte, Y. Zhang, J. Marc Raulot, M. Jeanne Philippe, C. Esling. A New Variant Selection Criterion for Twin Variants in Titanium Alloys (Part 1), Adv Eng Mater. 13 (2011) 1114-1121.

[22] S. Wang, C. Schuman, L. Bao, J.S. Lecomte, Y. Zhang, J.M. Raulot, M.J. Philippe, X. Zhao, C. Esling. Variant selection criterion for twin variants in titanium alloys deformed by rolling, Acta Mater. 60 (2012) 3912-3919.
[23] H. Qin, J.J. Jonas. Variant selection during secondary and tertiary twinning in pure titanium, Acta Mater. 75 (2014) 198-211.
[24] J.J. Jonas, S. Mu, T. Al-Samman, G. Gottstein, L. Jiang, Ė. Martin. The role of strain accommodation during the variant selection of primary twins in magnesium, Acta Mater. 59 (2011) 2046-2056.
[25] L. Wang, Y. Yang, P. Eisenlohr, T.R. Bieler, M.A. Crimp, D.E. Mason. Twin Nucleation by Slip Transfer across Grain Boundaries in Commercial Purity Titanium, Metall Mater Trans A. 41 (2009) 421-430.
[26] L. Wang, P. Eisenlohr, Y. Yang, T.R. Bieler, M.A. Crimp. Nucleation of paired twins at grain boundaries in titanium, Scr Mater. 63 (2010) 827-830.
[27] J. Luster, M.A. Morris. Compatibility of Dependence on Deformation in Two-Phase Ti-AI Alloys Microstructure and Orientation Relationships, Metall Mater Trans A. 26A (1995) 1745-1756.
[28] R. Xin, C. Guo, Z. Xu, G. Liu, X. Huang, Q. Liu. Characteristics of long {10-12} twin bands in sheet rolling of a magnesium alloy, Scr Mater. 74 (2014) 96-99.
[29] N. Bozzolo, L. Chan, A.D. Rollett. Misorientations induced by deformation twinning in titanium, J Appl Crystallogr. 43 (2010) 596-602.
[30] L. Bao, Y. Zhang, C. Schuman, J.-S. Lecomte, M.-J. Philippe, X. Zhao, C. Esling. Multiple twinning in pure hexagonal close-packed titanium, J Appl Crystallogr. 46 (2013) 1397-1406.
[31] R.J. Lederich, S.M.L. Sastry, J.E. O'neal, B.B. Rath. The effect of grain size on yield stress and work hardening of polycrystalline titanium at 295 K and 575 K, Mater Sci Eng. 33 (1978) 183-188.
[32] C.N. Tomé, R.A. Lebensohn, U.F. Kocks. A model for texture development dominated by deformation twinning: Application to zirconium alloys, Acta Metall. 39 (1991) 2667-2680.
[33] A. Ghaderi, M.R. Barnett. Sensitivity of deformation twinning to grain size in titanium and magnesium, Acta Mater. 59 (2011) 7824-7839.
[34] J.-J. Fundenberger, B. Beausir. Université de Lorraine - Metz, 2015, JTEX - Software for Texture Analysis, <http://jtex-software.eu/>.
[35] L.S. Toth, P. Gilormini, J.J. Jonas. Effect of rate sensitivity on the stability of torsion textures, Acta Metall 36 (1988) 3077-3091.
[36] A.A. Pochettino, N. Gannio, C.V. Edwards, R. Penelle. Texture and pyramidal slip in Ti, Zr and their alloys, Scr Metall. 27 (1992) 1859-1863.
[37] Y.N. Wang, J.C. Huang. Texture analysis in hexagonal materials, Mater Chem Phys. 81 (2003) 11-26.
[38] A. Styczynski, C. Hartig, J. Bohlen, D. Letzig. Cold rolling textures in AZ31 wrought magnesium alloy, Scr Mater. 50 (2004) 943-947.
[39] L. Capolungo, P.E. Marshall, R.J. McCabe, I.J. Beyerlein, C.N. Tomé. Nucleation and growth of twins in Zr: A statistical study, Acta Mater. 57 (2009) 6047-6056.
[40] K.E.K. Amouzou, T. Richeton, A. Roth, M.A. Lebyodkin, T.A. Lebedkina. Micromechanical modeling of hardening mechanisms in commercially pure α-titanium in tensile condition, Int J Plast. 80 (2016) 222-240.
[41] C.F. Gu, L.S. Toth, M. Hoffman. Twinning effects in a polycrystalline magnesium alloy under cyclic deformation, Acta Mater. 62 (2014) 212-224.
[42] R.A. Lebensohn, C.N. Tomé. A study of the stress state associated with twin nucleation and propagation in anisotropic materials, Philos Mag. 67 (1993) 187-206.
[43] P.A. Juan, S. Berbenni, M.R. Barnett, C.N. Tomé, L. Capolungo. A double inclusion homogenization scheme for polycrystals with hierarchal topologies: application to twinning in Mg alloys, Int J Plast. 60 (2014) 182-196.
[44] S. Mendelson. Dislocation Dissociations in hcp Metals, J Appl Phys. 41 (1970) 1893.
[45] S. Mendelson. Zonal dislocations and twin lamellae in h.c.p. metals, Mater Sci Eng. 4 (1969) 231-242.
[46] M.J. Philippe, M. Serghat, P.V. Houtte, C. Esling. Modelling of texture evolution for materials of hexagonal symmetry — II. application to zirconium and titanium α or near α alloys, Acta Metall. 43 (1995) 1619-1630.
[47] W.B. Hutchinson, M.R. Barnett. Effective values of critical resolved shear stress for slip in polycrystalline magnesium and other hcp metals, Scr Mater. 63 (2010) 737-740.

Figure captions

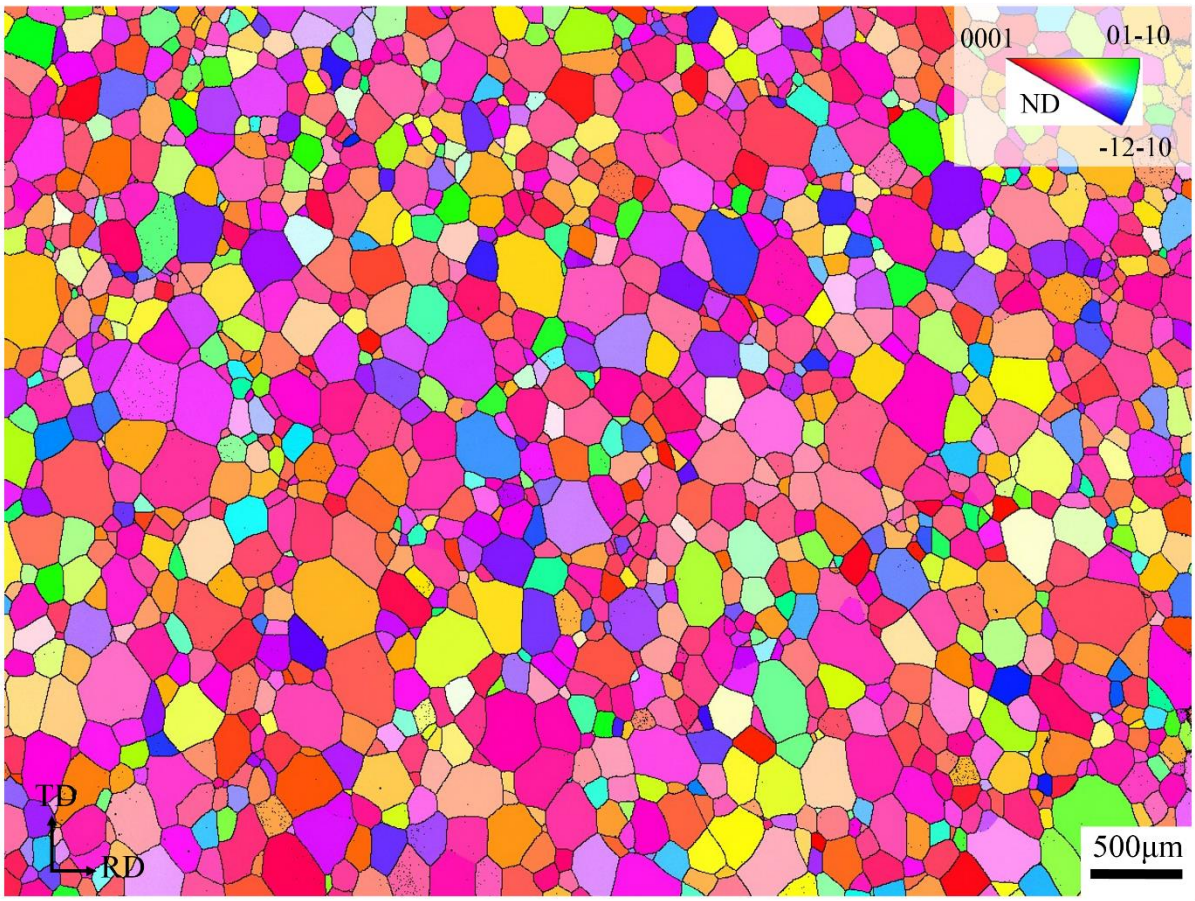

Fig. 1 IPF of the initial material with the projection of the ND axis.

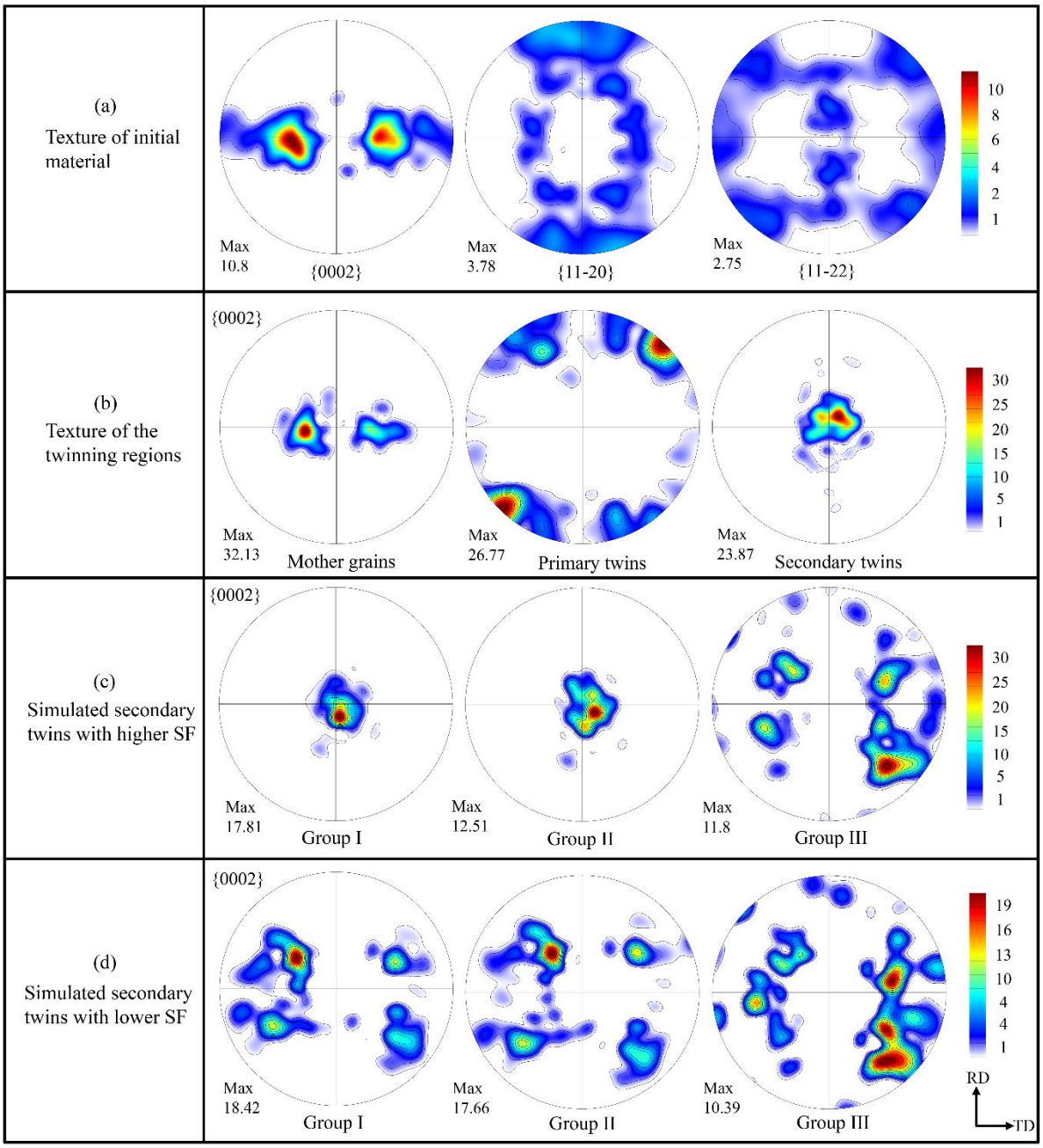

Fig. 2 (a) Texture of the initial material in {0002}, {11-22} and {10-10} pole figures, obtained from Fig. 1. (b) {0002} pole figures of parent grains, primary twins (where secondary twins were found) and secondary {10-12} twins from EBSD statistics. (c-d) Simulated secondary twins in {0002} pole figures using: (c) the highest Schmid factor-variant, (d) the second highest Schmid factor-variant, for each twinning group.

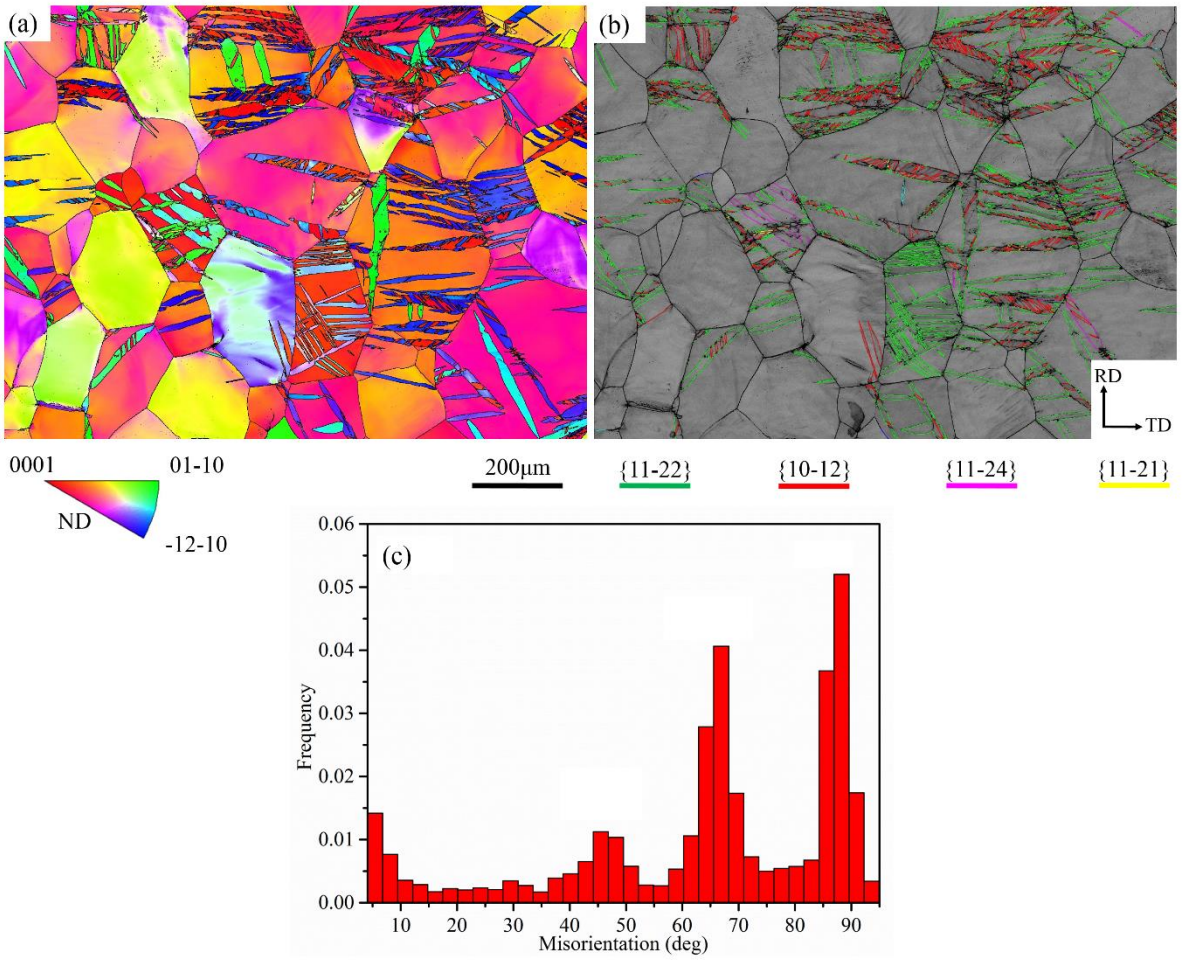

Fig. 3 A typical EBSD result of a sample compressed by 8.1% in IPF map (a) and in band contrast (b). Colour coded lines are used to identify the type of twins in (b). (c): The grain-to-grain misorientation angle distribution corresponding to the map in (a).

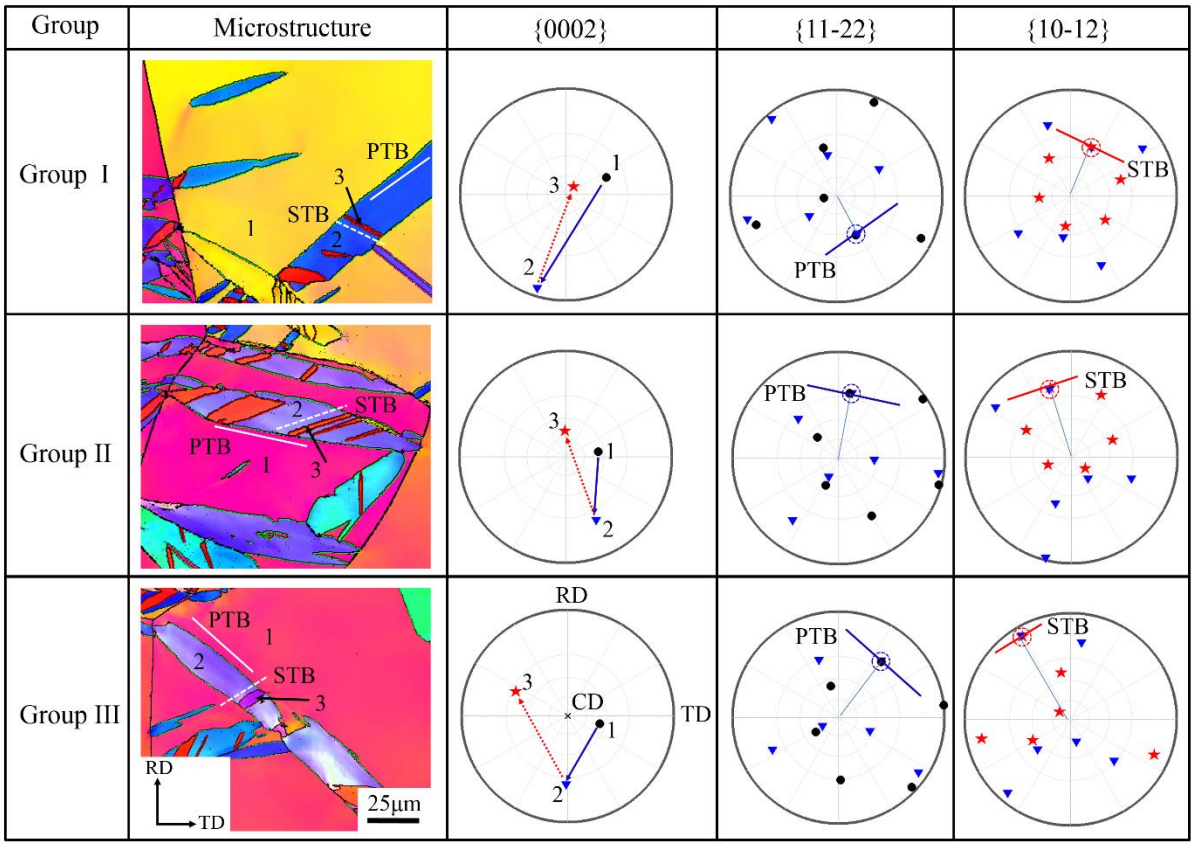

Fig. 4 EBSD examples of three secondary twinning group-variants listed in Table 4. The compression axis is indicated by CD. Lamellas 1, 2 and 3 represent the parent grains, primary {11-22} twins and secondary {10-12} twins, respectively. In the following {0002} pole figures, black solid points, blue triangles and red stars represent the c-poles of the parent grains, primary twins and secondary twins, respectively. In the {11-22} pole figures, the active {11-22} twin planes are showed by blue circles and the traces of primary twin boundaries (PTB) are indicated by blue lines. In the {10-12} pole figures, the active {10-12} twin planes are marked by red circles and the traces of secondary twin boundaries (STB) are displayed by red lines.

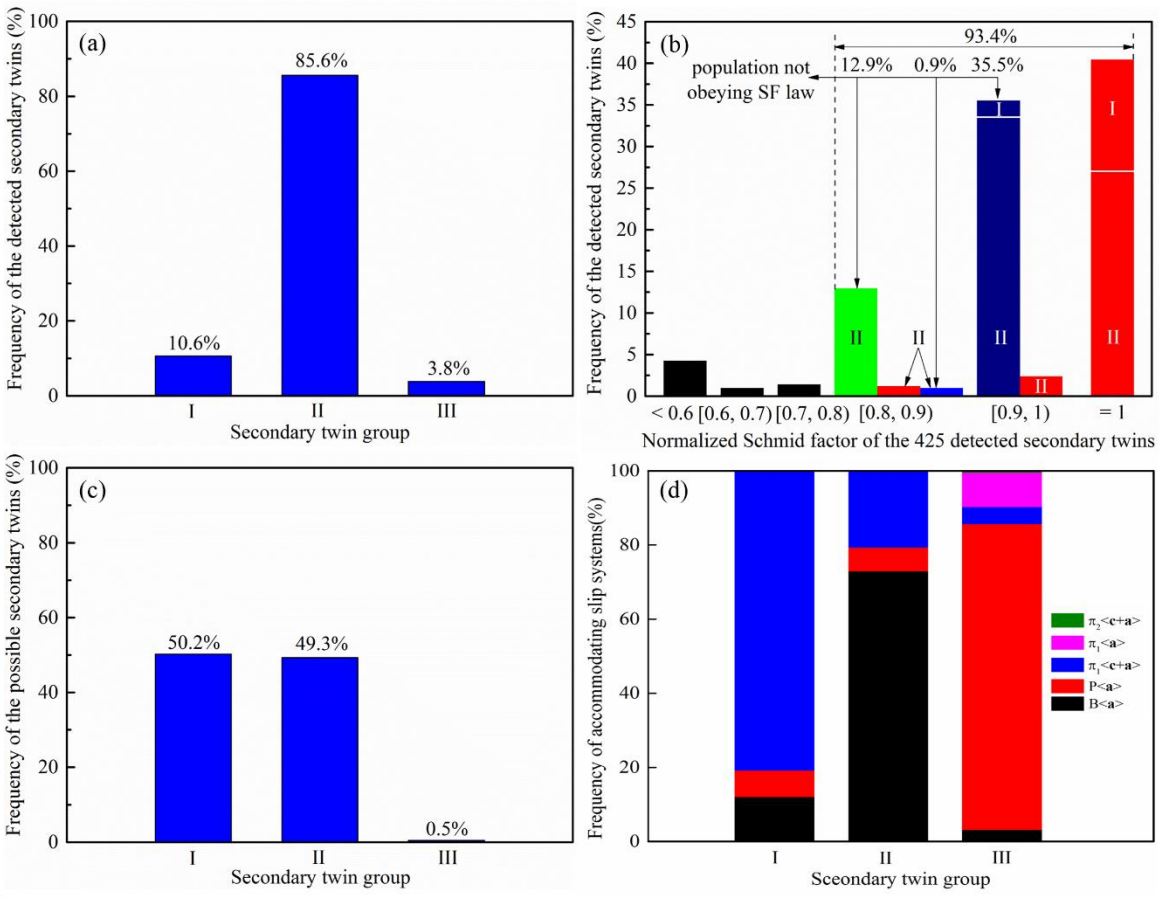

Fig. 5 (a) The observed group-frequency of 425 measured secondary twins. (b) Frequency distribution of the 425 measured secondary twins as a function of the normalized Schmid factor. Red colour means the highest SF variant is activated. Blue and green colours indicate variants with NSF < 1 in primary twins where the highest SF variant is absent. (c) Predicted frequency of the possible secondary twins using the highest and second highest Schmid factors. (d) Relative proportion of the different accommodating slip system families in the parent grains for the shears caused by secondary twins, by group-type.

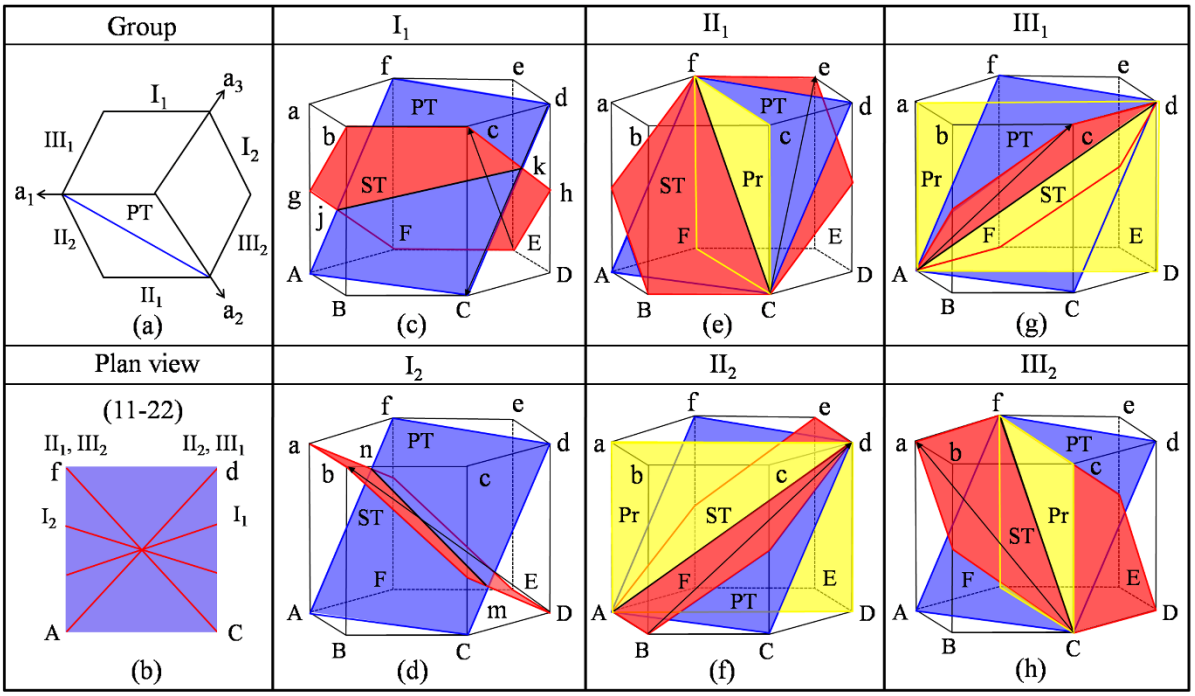

Fig. 6 Slip and twinning planes within primary twins. The primary (11-22) twin plane (purple) and the six secondary {10-12} twin planes (red) are shown. Each group contains two variants identified by the subscripts 1 and 2. The prismatic plane parallel to the common axis between primary and secondary twin planes is drawn in yellow. (a) Classification of six secondary twin planes into three groups. (b) The intersection lines of primary twin plane with six secondary twin planes in the (11-22) plan view. The other figures show the relations between primary and secondary twin systems and the common axes: (c) jk for I_1, (d) mn for I_2, (e) Cf for II_1, (f) Ad for II_2, (g) Ad for III_1, (h) Cf for III_2.

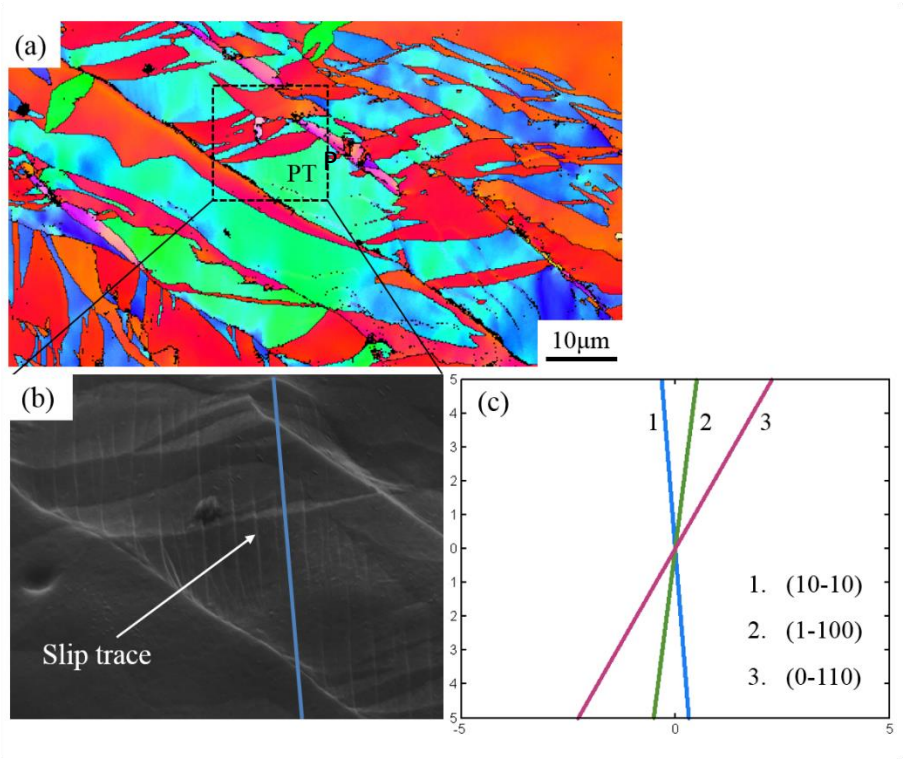

Fig. 7 (a): EBSD map from a pre-polished and subsequently deformed sample. (b): Secondary electron imaging of the region enlarged in (a). (c): Orientations of the possible three prismatic plane traces in the primary twin (the primary twin is identified by PT in the insert of (a)). The blue lines in (b) and (c) correspond to the prismatic trace for plane $(10\bar{1}0)$.

Table 1 Chemical composition of the commercially-pure titanium T40 used in the study.

element	H	C	N	O	Fe	Ti
Composition (wt. ppm)	3	52	41	1062	237	Balance

Table 2 Main deformation twin systems in titanium.

Type	Contraction twins		Tension twins	
K_1 plane	{11-22}	{11-24}	{10-12}	{11-21}
Rotation angle (deg)	~64	~77	~87	~35
Rotation axis	<-1100>	<-1100>	<1-210>	<-1100>

Table 3 The 36 possible combinations of secondary {10-12} extension twins and their minimum misorientations with respect to the parent grains. The same color indicates same group of secondary twin variants.

{11-22}-{10-12} double twins		Secondary {10-12} twin variants in primary twins					
		{10-12} <-1011>	{01-12} <0-111>	{-1102} <1-101>	{-1012} <10-11>	{0-112} <01-11>	{1-102} <-1101>
Primary {11-22} twin variants	{11-22}	<50-53>	<0-55-3>	<34-70>	<41-53>	<-1-45-3>	<-4-370>
	<11-2-3>	48.44°	48.44°	87.85°	41.34°	41.34°	87.85°
	{-12-12}	<3-740>	< 05-53>	<5-50-3>	<-47-30>	< -15-43>	<4-51-3>
	<-12-1-3>	87.85°	48.44°	48.44°	87.85°	41.34°	41.34°
	{-2112}	<5-1-4-3>	<7-4-3 0>	<-5503>	<50-5-3>	<-7340>	< -5413>
	<-211-3>	41.34°	87.85°	48.44°	48.44°	87.85°	41.34°
	{-1-122}	<-4-153>	<14-5-3>	<43-70>	<-5053>	<05-5-3>	<-3-470>
	<-1-12-3>	41.34°	41.34°	87.85°	48.44°	48.44°	87.85°
	{1-212}	<4-730>	<1-543>	<-45-1-3>	< -37-40>	<0-553>	<-550-3>
	<1-21-3>	87.85°	41.34°	41.34°	87.85°	48.44°	48.44°
	{2-1-12}	<-505-3>	<7-3 -4 0>	<5-4-13>	<-5143>	<-7340>	<5-503>
	<2-1-1-3>	48.44°	87.85°	41.34°	41.34°	87.85°	48.44°

Table 4 Classification of secondary twin variants from Table 3 into three groups.

Group	Axis-angle (minimum)	Number of variants
I	<5 -1 -4 3> 41.34°	12
II	<-5 5 0 3> 48.44°	12
III	<7 -4 -3 0> 87.85°	12

Table 5 Slip systems and the critical resolved shear stress in pure titanium (from [40]).

Slip systems	{10-10} <-12-10>	{0001} <1-210>	{10-11} <-12-10>	{10-11} <2-1-1-3>	{11-22} <11-2-3>
Notation	P<**a**>	B<**a**>	Π_1<**a**>	Π_1<**c**+**a**>	Π_2<**c**+**a**>
CRSS / MPa	141	254	197	338	353

Table 6 Angles between primary {11-22} and secondary {10-12} twin planes within the three groups.

Group	I	II	III
Angle between plane normals (deg)	84.1	27.4	66.9

Table 7 The Miller-Bravais indices of the common direction between a primary (11-22) twin, the six secondary twins as well as the corresponding prismatic plane for the three secondary twin groups.

Primary twin variant	(11-22) [11-2-3]					
Group	I		II		III	
Secondary twin variants	I_1 (0-112)	I_2 (-1012)	II_1 (01-12)	II_2 (10-12)	III_1 (1-102)	III_2 (-1102)
Common axis	[8 -10 2 3]	[-10 8 2 3]	[-4 2 2 3]	[2 -4 2 3]	[-4 2 2 3]	[2 -4 2 3]
Prismatic plane	-	-	(10-10)	(01-10)	(01-10)	(10-10)